THE JOURNAL OF PHYSICAL CHEMISTRY Letters

Letter

pubs.acs.org/JPCL

# Minimal Model of Quantum Kinetic Clusters for the Energy-Transfer Network of a Light-Harvesting Protein Complex

Jianlan Wu,*[,†] Zhoufei Tang,[†] Zhihao Gong,[†] Jianshu Cao,[‡] and Shaul Mukamel[¶]

[†]Physics Department, Zhejiang University, 38 ZheDa Road, Hangzhou, Zhejiang 310027, China

[‡]Department of Chemistry, Massachusetts Institute of Technology, 77 Massachusetts Avenue, Cambridge, Massachusetts 02139, United States

[¶]Department of Chemistry, University of California, Irvine, California 92697, United States

Supporting Information

**ABSTRACT:** The energy absorbed in a light-harvesting protein complex is often transferred collectively through aggregated chromophore clusters. For population evolution of chromophores, the time-integrated effective rate matrix allows us to construct quantum kinetic clusters quantitatively and determine the reduced cluster−cluster transfer rates systematically, thus defining a minimal model of energy-transfer kinetics. For Fenna−Matthews−Olson (FMO) and light-havrvesting complex II (LCHII) monomers, quantum Markovian kinetics of clusters can accurately reproduce the overall energy-transfer process in the long-time scale. The dominant energy-transfer pathways are identified in the picture of aggregated clusters. The chromophores distributed extensively in various clusters can assist a fast and long-range energy transfer.

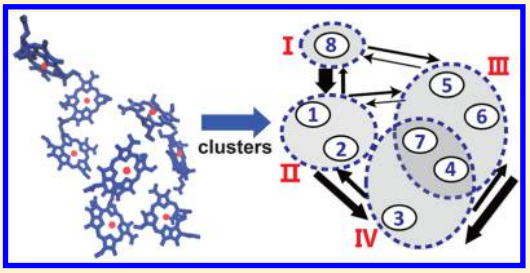


With almost unity transfer efficiency, the early energy-transfer step in light-harvesting protein complexes has attracted great interest from both experimental and theoretical perspectives.[1] The two-dimensional electronic spectroscopy technique can explore major energy-transfer pathways from the detailed time-resolved spectroscopic studies[2,3] and has demonstrated long-lived quantum coherence in various light-harvesting systems, suggesting its role in the energy-transfer process.[4−6] Theoretical studies of energy transfer are carried out under the quantum dynamic framework, beyond the conventional incoherent hopping picture. The bath-induced quantum dissipation is found to result in an optimal transfer efficiency in the intermediate dissipation regime,[7−12] which is close to the physiological condition of light-harvesting protein complexes.

The light-harvesting protein complexes are rich in their spatial structures and energy-transfer dynamics. The bacteriochlorophyll (BChl) molecules in light-harvesting I (LHI) and II (LHII) complexes of purple bacteria are organized into symmetric rings. On the short-time scale, the intraring energy transfer can behave coherently due to symmetric and non-negligible interactions between BChl molecules.[13,14] On the long-time scale, the inter-ring energy transfer becomes incoherent, and multichromophoric Förster resonance energy transfer (MC-FRET) is proposed for calculating the dynamics of aggregates.[15−17] For many other light-harvesting systems, the spatial arrangement of chromophores is not symmetric, but aggregated clusters can be still formed because interactions between chromophores can be partitioned into groups. The overall energy-transfer process is separated into fast intracluster and slow intercluster dynamics. For example, the major two-step pathway in an eight-BChl Fenna−Matthews−Olson (FMO) monomer can be approximated in a three-cluster system, where BChls 1 and 2 are simplified into a pre-equilibrated dimer (see Figure 1a).[8,18,19] In the light-harvesting complex II (LHCII) system, previous studies have suggested three spatial clusters on the stromal layer, chlorophylls (Chls) a602-a603, a610-a611-a612, and b601′-b608-b609, and two clusters on the lumenal layer, Chls b606-b607-b605-a604 and a613-a614.[20−22]

The characterization of clusters in previous studies is mainly based on the spatial separation, which is a static picture and structure-based. However, for an energy-transfer network, one site can extensively interact with multiple sites as a bridge connecting various spatially separated clusters.[6] The fast, long-range energy transfer assisted by such a hub site modulates energy-transfer pathways in light-harvesting protein complexes. To illustrate this important contribution of delocalized quantum coherence, we will treat each cluster as a linear combination of sites with fractional coefficients in this Letter. As demonstrated in two example systems, FMO and LHCII, an effective site−site rate matrix helps us construct clusters systematically and quantitatively, and quantum Markovian kinetics of clusters can reproduce the overall population evolution and the equilibrium distribution accurately. This method can also identify relevant hub sites with large partition coefficients in connecting clusters. These hub sites are crucial for maintaining the stability of the energy-transfer network.

**Received:** February 2, 2015
**Accepted:** March 19, 2015
**Published:** March 19, 2015

ACS Publications © 2015 American Chemical Society



DOI: 10.1021/acs.jpclett.5b00227
*J. Phys. Chem. Lett.* 2015, 6, 1240−1245

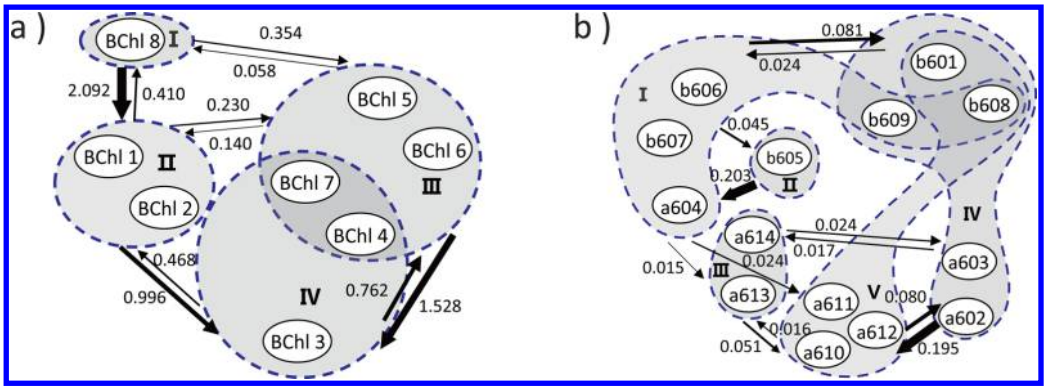


**Figure 1.** Schematic pictures of (a) four quantum kinetic clusters in the 8-site FMO and (b) five quantum kinetic clusters in the 14-site LHCII. Each cluster is labeled and identified by a gray ellipse. The major reduced cluster−cluster transfer rates are provided.

For an energy-transfer network in light-harvesting systems, the total Hamiltonian is given by $H_{tot} = H_S + H_B + H_{SB}$, where $H_S$ and $H_B$ represent the bare Hamiltonians of the system and bath, respectively. Within the single-excitation manifold, the system Hamiltonian is written as $H_S = \sum_n \epsilon_n |n\rangle\langle n| + \sum_{n\neq m} J_{nm} |n\rangle\langle m|$, where $\epsilon_n$ defines the electronic excitation energy at site $n$ and $J_{nm}$ defines the electronic coupling between sites $n$ and $m$. The system−bath interaction $H_{SB}$ is approximated in a bilinear form, $H_{SB} = \sum_n |n\rangle\langle n| B_n$, where $B_n$ is a bath operator. Under a system−bath factorized initial condition, we assume an incoherent site population preparation for the system. The time evolution of the system population $P(t)$ reduced from full quantum dynamics rigorously follows a time-convolution equation

$$\dot{P}(t) = -\int_0^t \mathcal{K}(t-\tau)P(\tau)\,d\tau \tag{1}$$

where $\mathcal{K}(t)$ is the non-Markovian rate kernel matrix. Despite relevant non-Markovian features in the short-time scale, the quantum Markovian kinetics approximately describe the population evolution, $\dot{P}(t) = -KP(t)$, where the time integration

$$K = \int_0^\infty \mathcal{K}(t)\,dt \tag{2}$$

leads to effective rates between different chromophores quantitatively.[23] The effective rate matrix $K$ can be obtained by the block matrix inversion method in the hierarchy equation of motion (HEOM).[24,25]

Our first example is the FMO protein complex in green sulfur bacteria. Recent experiments have revealed the eighth BChl molecule locating on the surface of the FMO protein complex. The 8-site Hamiltonian from refs 8 and 19 is applied to the FMO monomer. The system−bath coupling is modeled by the Debye spectral density, $J(\omega) = (2\lambda/\pi)\omega\omega_D/(\omega^2 + \omega_D^2)$, with the reorganization energy $\lambda = 35$ cm$^{-1}$ and the cutoff frequency $\omega_D^{-1} = 50$ fs.[7−9] At room temperature ($T = 300$ K), the high-$T$ approximation leads to a single-exponential decay for the bath−time correlation function $C(t)$. Because energy is transported from the chlorosome, we set the initial population at BChl 8. The full quantum dynamics is calculated using the HEOM, which is numerically converged at the hierarchic truncation order of $H = 7$. The resulting population dynamics is plotted in Figure 2, consistent with previous studies.[8,19] Next, we extract the major energy-transfer pathways. The population initially localized at BChl 8 is first transferred to BChl 1 due to

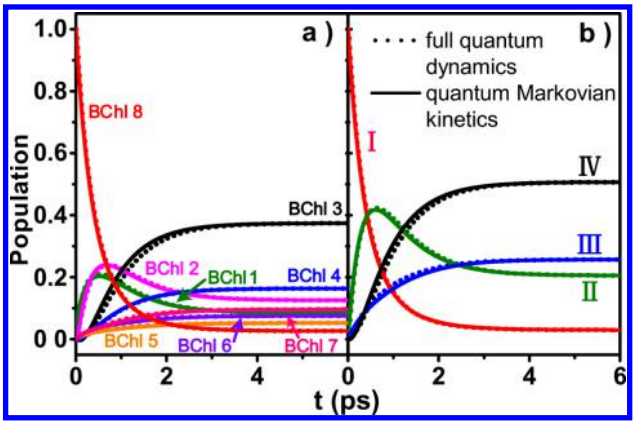


**Figure 2.** Time evolution curves of the 8-site FMO with the initial population at BChl 8: (a) the site populations; (b) the cluster populations. The dotted and solid lines are calculated by the non-Markovian HEOM and Markovian kinetics, respectively. The results of each BChl site in (a) and each kinetic cluster in (b) are labeled and shown in a specific color.

their relatively strong electronic coupling strength (37.5 cm$^{-1}$). A much stronger coupling strength (−97.9 cm$^{-1}$) quickly synchronizes the population of BChls 1 and 2, and these two chromophores behave like a dimer.[8,18,19,26,27] After the population of the dimer reaches its maximum value within 1 ps, the population starts to accumulate at BChl 3 with the lowest excitation energy. The other chromophores also gradually increase their populations. The FMO monomer reaches full equilibrium in less than 5 ps.

Following the block matrix inversion method, we calculate the time-integrated rate matrix $K$ defined in eq 2 (see the Supporting Information). This effective rate matrix is independent of the initial system population. As shown in Figure 2, Markovian kinetics, $P(t) = \exp(-Kt)P(0)$, agree with non-Markovian dynamics for $t > 2$ ps, predicting exactly the same equilibrium population. Only a small non-Markovian effect can be observed for $t < 2$ ps. The energy-transfer rates are not evenly distributed between different pairs of chromophores, and the population evolution exhibits a time scale separation; sites under fast local equilibrium aggregate into quantum kinetic clusters, and the excitation energy is transferred collectively through the clusters, especially in the long-time scale. From Markovian kinetics, the population of each $j$th BChl molecule is written as


DOI: 10.1021/acs.jpclett.5b00227
J. Phys. Chem. Lett. 2015, 6, 1240−1245

$$P_j(t) = \sum_{k=0}^{7} c_{jk} \exp(-\gamma_k t) \tag{3}$$

where $\gamma_k$ is the $k$th eigenvalue of the rate matrix $K$, satisfying $\gamma_0(=0) < \gamma_1 < \cdots < \gamma_7$. The coefficient $c_{j0}$ associated with the zero eigen rate is the equilibrium population $p_j^{eq}$ of the $j$th BChl molecule. For the final site, BChl 3, the coefficients $c_{3k(\leq 3)}$ associated with the four smallest eigen rates $\gamma_{k(\leq 3)}$ are at least 30 times larger than the other four coefficients (see eq 5 of the Supporting Information). Thus, a four-cluster minimal model can be constructed to represent the energy-transfer network if we are mainly interested in long-time dynamics with population accumulation at BChl 3.

To separate the fast and slow components of population, we introduce a linear transformation to combine the population of each $i$th cluster as $P_i^C(t) = \sum_j S_{ij} P_j(t) = \sum_{j,k} S_{ij} c_{jk} \exp(-\gamma_k t)$, where the elements $S_{ij}$ of the transformation matrix need to be determined. For the four quantum kinetic clusters, the partition coefficients associated with fast eigen rates must vanish, that is, $\sum_j S_{ij} c_{jk} = 0$ for $k > 3$. The system Hamiltonian provides a crude estimation of kinetic clusters. For instance, the weak couplings between BChl 8 and the other sites suggest a single-site cluster. Our cluster partition procedure (see more details in the Supporting Information) is described as follows: (i) For each cluster, we keep five sites and neglect the three least relevant sites based on the electronic couplings. Each of the initial (BChl 8) and final (BChl 3) sites is assigned to an individual cluster, while a dominant site is selected as the reference site in each intermediate cluster. (ii) For each cluster, we set a unity partition coefficient for the reference site, and the remaining four partition coefficients are determined relatively by solving the four-equation array, $\sum_j S_{ij} c_{jk} = 0$ $(k = 4-7)$, from fast kinetics. (iii) The normalization condition $\sum_{i=1}^{4} S_{ij} = 1$ resolves the transformation matrix $S$ uniquely. Consequently, we construct the following four quantum kinetic clusters

$$P_{\mathrm{I}}^C(t) = P_8(t) + 0.06P_1(t)$$

$$P_{\mathrm{II}}^C(t) = 0.92P_1(t) + 0.96P_2(t) + 0.06P_5(t) + 0.07P_6(t)$$

$$P_{\mathrm{III}}^C(t) = 0.93P_5(t) + 0.93P_6(t) + 0.62P_7(t) + 0.47P_4(t)$$

$$P_{\mathrm{IV}}^C(t) = P_3(t) + 0.53P_4(t) + 0.37P_7(t) + 0.07P_2(t)$$

where only components with $|S_{ij}| \geq 0.05$ are shown for clarity. Although the cluster construction exhibits flexibility, our approach assisted by the system Hamiltonian separation captures physically appealing clusters in the minimal model. The partition coefficients for the fast population kinetics can be similarly calculated. The transformed rate matrix $K' = SKS^{-1}$ becomes block diagonal, with two $4 \times 4$ submatrices separating fast and slow eigen rates. The reduced rate matrix $K^C$ for the quantum kinetic clusters is given by

$$K^C = \begin{pmatrix} 2.401 & -0.410 & -0.058 & 0.053 \\ -2.092 & 1.635 & -0.140 & -0.468 \\ -0.354 & -0.230 & 1.725 & -0.762 \\ 0.044 & -0.996 & -1.528 & 1.176 \end{pmatrix} \mathrm{ps}^{-1} \tag{4}$$

The eigen rates of $K^C$ are exactly the same as those for the four relevant ones of the site−site rate matrix $K$ (see eq 4 in the Supporting Information). The quantum kinetic clusters in FMO and their dominant effective rates are plotted in Figure 1a. We observe a major energy-transfer pathway, clusters I (BChl 8) → II (BChls 1 and 2) → IV (BChls 3, 4, and 7), whereas cluster III (BChls 5, 6, 4, and 7) modulates the energy-transfer process through a minor pathway, clusters I → III → IV. Next, we plot the cluster population evolution from the Markovian kinetics, using $P^C(t) = \exp(-K^C t)P^C(0)$, compared with the result of the non-Markovian HEOM in Figure 2b. For kinetic clusters, the results of Markovian kinetics and non-Markovian dynamics agree well with each other. The major pathway is revealed by the subsequent population accumulation along clusters I → II → IV. The dominant intermediate, cluster II, is identified with its maximum population within 1 ps. The two-step energy-transfer scenario has been proposed previously,[8,19] and our current work provides a more systematic and quantitative description using the concept of quantum kinetic clusters.

Our constructed clusters are not limited to a special initial state at BChl 8. As an example, we prepare the initial population at BChl 6 and calculate the new population evolution. Figure 3 demonstrates that Markovian kinetics

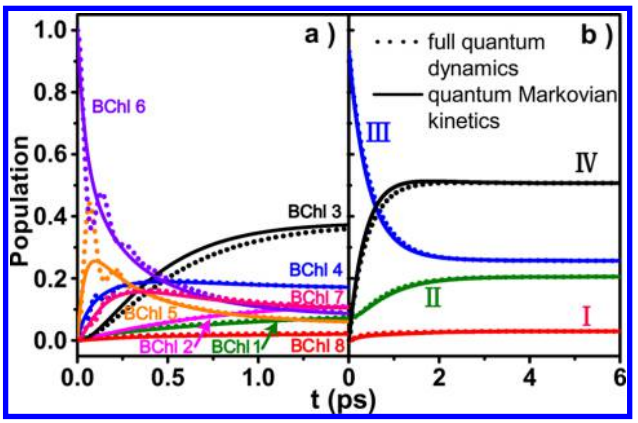


**Figure 3.** Time evolution curves of the 8-site FMO with the initial population at BChl 6: (a) the site populations; (b) the cluster populations. The dotted and solid lines are calculated by the non-Markovian HEOM and Markovian kinetics, respectively. The results of each BChl site in (a) and each kinetic cluster in (b) are labeled and shown in a specific color.

from the same cluster rate matrix in eq 4 agree well with the exact non-Markovian dynamics, although the site rate matrix fails to reproduce a short-time quantum oscillation of BChls 6 and 5. The time evolution of aggregated clusters can be reliably described by quantum Markovian kinetics. With the same cluster rate matrix, the energy-transfer pathway changes with the initial condition. With the initial population at BChl 6, the pathway, clusters III → IV, becomes dominant, consistent with the previous site-based pathway studies in the 7-site FMO system.[9,18,26,27] The "hub" site, BChl 4, extensively distributed in clusters III and IV controls the population flow along the major energy-transfer pathway and realizes a fast (∼1 ps) long-range energy transfer from BChls 6 to 3. BChl 4 is crucial for the stability of the FMO network, and a permanent damage on this hub site can significantly delay the energy-transfer process (∼5 ps) when the initial population is at BChl 6.

Our second example is the LHCII, which is an important antenna protein complex, initiating the excitation energy-transfer process in the photosystem II (PSII). Each LHCII monomer is composed of 14 chlorophyll (Chl) molecules, 8 Chl-a and 6 Chl-b. The effective 14-site Hamiltonian is taken from ref 20. The model bath spectral density includes a low-


DOI: 10.1021/acs.jpclett.5b00227
J. Phys. Chem. Lett. 2015, 6, 1240−1245

frequency Debye mode and 48 high-frequency Brownian oscillator modes. For simplicity, we only focus on the low-frequency Debye spectral density ($\lambda = 85\ \mathrm{cm}^{-1}$ and $\omega_D^{-1} = 53.08$ fs) and ignore all of the high-frequency components. This approximation neglects population dynamics from resonant electron−phonon coupling,[20−22,28,29] which is however acceptable considering our main purpose of demonstrating aggregated kinetic clusters. LHCII is a membrane protein complex, with both stormal and lumenal sides. Here, we set the initial population at Chl b606 on the lumenal side and inspect the population accumulation at Chls a610-a611-a612 on the stormal side. With the high-temperature approximation for $T = 300$ K, the HEOM is truncated at $H = 6$, where the average numerical error of energy-transfer rates is less than 3%.[30]

The population evolutions from the non-Markovian HEOM and the Markovian kinetics of the time-integrated rate matrix (see the Supporting Information) are plotted in Figure 4. The

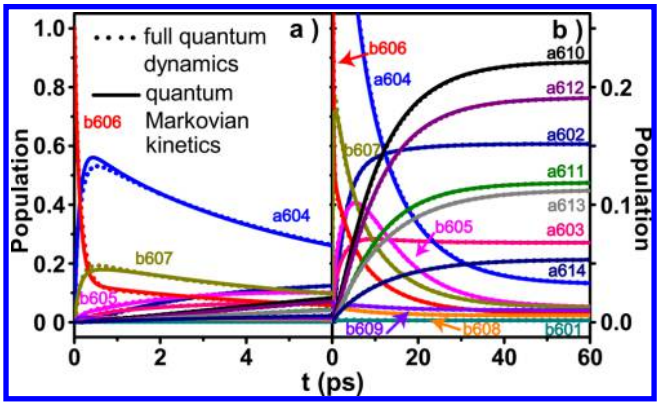


**Figure 4.** Site population evolution curves of the 14-site LHCII with the initial population at Chl b606. Panels (a) and (b) represent short-time and long-time results, respectively. The dotted and solid lines are calculated by the non-Markovian HEOM and Markovian kinetics, respectively. The result of each Chl site is labeled and shown in a specific color.

result of population dynamics is qualitatively consistent with previous studies.[20−22,28,29] These two approaches lead to almost the same population dynamics, except for observable differences at short times. The dynamical behaviors in the two panels of Figure 4 reveal a strong time scale separation.[20−22,28,29] In the short-time regime (<0.5 ps), population is quickly transferred from Chl b606 to Chls a604 (interband) and b607 (intraband) due to their strong interactions. After populations of Chls a604 and b07 reach maximum values, these three sites on the lumenal side are in local equilibrium. Subsequently, the population slowly diffuses to the entire LHCII monomer and accumulates on the stromal side. In the long-time regime, population dynamics become much more complicated, involving multiple energy-transfer pathways.

We now apply our approach used in FMO to construct quantum kinetic clusters in the LHCII monomer. By expanding the multiexponential functions of Markovian kinetics, we find that the population evolution of the final sites, Chls a610-a611-a612, are dominated by the five smallest eigen decay rates (see eqs 10−12 of the Supporting Information). The 14-site LHCII monomer is kinetically reduced into a five-cluster minimal model. Following the same procedure in FMO, we set the initial cluster of Chl b606 and the final cluster of Chls a610-a611-a612. As for the intermediate clusters, Chl b605 must be isolated to avoid an unphysically large partition coefficient in other clusters. Unlike previous studies,[20−22] Chls b601-b608-b609 do not form an isolated kinetic cluster due to their extensive interactions with multiple clusters. After solving the relative coefficients and applying the normalization condition, the five quantum kinetic clusters (see Figure 1b) are determined as follows

$$P_{\mathrm{I}}^{\mathrm{C}}(t) = 1.09P_4(t) + P_6(t) + 0.99P_7(t) + 0.13P_8(t) + 0.10P_9(t)$$

$$P_{\mathrm{II}}^{\mathrm{C}}(t) = P_5(t)$$

$$P_{\mathrm{III}}^{\mathrm{C}}(t) = 0.99P_{13}(t) + 0.99P_{14}(t)$$

$$P_{\mathrm{IV}}^{\mathrm{C}}(t) = 0.97P_2(t) + 0.96P_3(t) + 0.87P_9(t) + 0.76P_1(t) + 0.57P_8(t) - 0.05P_4(t)$$

$$P_{\mathrm{V}}^{\mathrm{C}}(t) = P_{10}(t) + 1.02P_{11}(t) + 1.02P_{12}(t) + 0.29P_8(t) + 0.21P_1(t)$$

where only components with $|S_{ij}| \geq 0.05$ are shown for clarity. The effective rate matrix for this five-cluster system is given by

$$K^{\mathrm{C}} = \begin{pmatrix} 0.164 & -0.203 & -0.006 & -0.024 & -0.002 \\ -0.045 & 0.218 & 0.000 & 0.001 & 0.000 \\ -0.015 & -0.002 & 0.081 & -0.017 & -0.016 \\ -0.081 & -0.007 & -0.024 & 0.236 & -0.080 \\ -0.024 & -0.006 & -0.051 & -0.195 & 0.097 \end{pmatrix} \mathrm{ps}^{-1} \quad (5)$$

The quantum kinetic clusters in LHCII and their dominant effective rates are plotted in Figure 1b. As shown in Figure 4, the short-time population evolution (<0.5 ps) mainly occurs in cluster I (Chls a604-b606-b607) for the local equilibrium. Next, we plot the cluster population evolution from non-Markovian dynamics and Markovian kinetics in Figure 5. The results of these two approaches are almost identical, except for very small differences in the short-time regime (<1 ps). The overall dynamics of clusters in the LHCII monomer can be accurately described by quantum Markovian kinetics. Following the

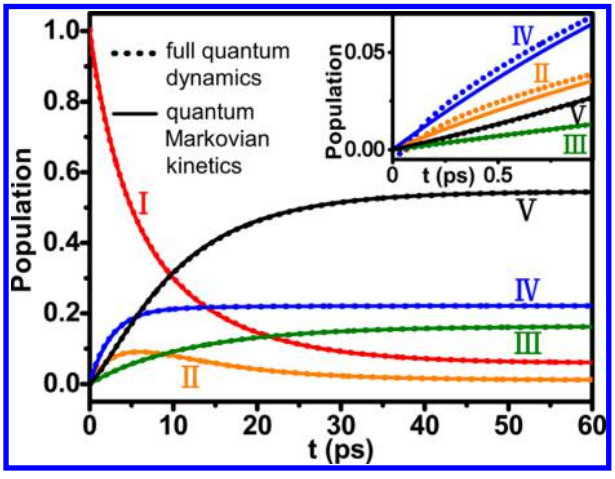


**Figure 5.** Cluster population evolution curves in the 14-site LHCII with the initial population at Chl b606. The short-time (<1 ps) results are magnified in the inset. The dotted and solid lines are calculated by the non-Markovian HEOM and Markovian kinetics, respectively. The result of each cluster is labeled and shown in a specific color.



DOI: 10.1021/acs.jpclett.5b00227
J. Phys. Chem. Lett. 2015, 6, 1240−1245

population flux analysis technique (see the Supporting Information), the major pathway is a sequential energy transfer of clusters I → IV (∼8 ps) → V (∼15 ps after initialized around 1 ps). The large ratio of $k_{V\leftarrow I}/k_{I\leftarrow V}$ leads to a minor but unidirectional pathway, clusters I → V (∼10 ps). The intermediate interaction between Chls b606 and b605 allows a fast energy transfer, clusters I → II, but the population accumulated at the isolated cluster II is mainly transferred back to cluster I after 6.5 ps to facilitate the two pathways above. Cluster III (Chls a613-a614) can transfer its population to cluster V with an intermediate rate (0.048 $ps^{-1}$), but its weak interaction with clusters I and IV determines that cluster III plays a minor role in the overall energy-transfer process.

The above construction of quantum kinetic clusters and the population evolution are qualitatively consistent with previous studies, especially on the major energy-transfer pathways.[20−22] In our approach, the two major hub sites, Chls b608 and b609, are extensively distributed into three clusters, I, IV, and V, controlling the population flow. For example, the population flowed from Chl b606 is almost 100% transferred to Chls a602-a603 through the intermediate site Chl b609 (see the Supporting Information). The same behavior occurs for the population flow of Chls b606 → b608 → a610. The major cluster pathway, I → IV → V, in the minimal model corresponds to the pathway Chls b606-(b607-a604) → b609-(b608-b601) → a603-a602 → a610-a611-a612 in previous studies.[20−22] Similarly, the minor cluster pathway, I → V, corresponds to the pathway Chls b606-(b607-a604) → b608-(b609-b601) → a610-(a611-a612). For the subnetwork of clusters I, IV, and V, the removal of Chls b608 and b609 can significantly delay the overall transfer process from 10 to 70 ps. The minimal model can thus identify the importance of these two hub sites in the whole energy-transfer network. With high-frequency bath modes, the cluster structure and the energy-transfer pathways are qualitatively consistent but require a quantitative modification.

Artificial and natural photosynthetic systems take advantage of the Coulombic interaction to enhance the stability and efficiency of energy transfer. The excitation electronic coupling results in the delocalization of the wave function and hence the formation of coherent clusters that function as the basic units of thermal hopping. In this Letter, we propose a strategy to construct these clusters from dynamic trajectories instead of static structure and thus rigorously reproduce the energy flow in between clusters. With the time-integrated effective site−site rate matrix from full quantum dynamics, we apply the block diagonalization approach to construct quantum kinetic clusters in a minimal model. The proposed approach is demonstrated in two example systems, 8-site FMO and 14-site LHCII monomers, which are reduced to four- and five-cluster networks, respectively. The quantum Markovian kinetics of aggregated clusters can accurately reproduce the same long-time evolution as that from the full non-Markovian quantum dynamics. The major energy-transfer pathways are determined in the cluster description. More importantly, our method reveals that energy is transferred collectively through kinetic clusters, assisted by extensive interactions of hub chromophores. This minimal model analysis can be applied to other artificial and natural photosynthetic systems.[31,32] For complex multisite light-harvesting systems, our investigation suggests that full quantum dynamics may be replaced by coarse-grained methods based on kinetic clusters determined self-consistently.

## ■ ASSOCIATED CONTENT

### Supporting Information

Time-integrated effective rate matrix of the 8-site FMO, quantum kinetic cluster construction in the 8-site FMO, time-integrated effective rate matrix of the 14-site LHCII, quantum kinetic cluster construction in the 14-site LHCII, and Markovian population flux in the 14-site LHCII. This material is available free of charge via the Internet at http://pubs.acs.org.

## ■ AUTHOR INFORMATION

### Corresponding Author

*E-mail: jianlanwu@zju.edu.cn.

### Notes

The authors declare no competing financial interest.

## ■ ACKNOWLEDGMENTS

The work reported here is supported by the Ministry of Science and Technology of China (MOST-2014CB921203) and the National Nature Science Foundation of China (NSFC-21173185).

## ■ REFERENCES

(1) Renger, T.; May, V.; Kühn, O. Ultrafast Excitation Energy Transfer Dynamics in Photosynthetic Pigment−Protein Complexes. *Phys. Rep.* **2001**, *343*, 137−254.
(2) Mukamel, S. *Principles of Nonlinear Optics and Spectroscopy*; Oxford University Press: New York, 1995.
(3) Cheng, Y. C.; Fleming, G. R. Dynamics of Light Harvesting in Photosynthesis. *Annu. Rev. Phys. Chem.* **2009**, *60*, 241−262.
(4) Engel, G. S.; Calhoun, T. R.; Read, E. L.; Ahn, T. K.; Mančal, T.; Cheng, Y. C.; Blankenship, R. E.; Fleming, G. R. Evidence for Wavelike Energy Transfer through Quantum Coherence in Photosynthetic Systems. *Nature* **2007**, *446*, 782−786.
(5) Collini, E.; Wong, C. Y.; Wilk, K. E.; Curmi, P. M. G.; Brumer, P.; Scholes, G. D. Coherently Wired Light-Harvesting in Photosynthetic Marine Algae at Ambient Temperature. *Nature* **2010**, *463*, 644−647.
(6) Chenu, A.; Scholes, G. D. Coherence in Energy Transfer and Photosynthesis. *Annu. Rev. Phys. Chem.* **2015**, *66*, 69−96.
(7) Wu, J. L.; Liu, F.; Shen, Y.; Cao, J. S.; Silbey, R. J. Efficient Energy Transfer in Light-Harvesting Systems, I: Optimal Temperature,Reorganization Energy and Spatial−Temporal Correlations. *New J. Phys.* **2010**, *12*, 105012.
(8) Moix, J.; Wu, J. L.; Huo, P. F.; Coker, D.; Cao, J. S. Efficient Energy Transfer in Light-Harvesting Systems, III: The Influence of the Eighth Bacteriochlorophyll on the Dynamics and Efficiency in FMO. *J. Phys. Chem. Lett.* **2011**, *2*, 3045−3052.
(9) Wu, J. L.; Liu, F.; Ma, J.; Silbey, R. J.; Cao, J. S. Efficient Energy Transfer in Light-Harvesting Systems: Quantum−Classical Comparison, Flux Network, and Robustness Analysis. *J. Chem. Phys.* **2012**, *137*, 174111.
(10) Wu, J. L.; Silbey, R. J.; Cao, J. S. Generic Mechanism of Optimal Energy Transfer Efficiency: A Scaling Theory of the Mean First-Passage Time in Exciton Systems. *Phys. Rev. Lett.* **2013**, *110*, 200402.
(11) Rebentrost, P.; Mohseni, M.; Kassal, I.; Lloyd, S.; Aspuru-Guzik, A. Environment-Assisted Quantum Transport. *New J. Phys.* **2009**, *11*, 033003.
(12) Plenio, M. B.; Huelga, S. F. Dephasing-Assisted Transport: Quantum Networks and Biomolecules. *New J. Phys.* **2008**, *10*, 113019.
(13) Hu, X.; Ritz, T.; Damjanovic, A.; Schulten, K. Pigment Organization and Transfer of Electronic Excitation in the Photosynthetic Unit of Purple Bacteria. *J. Phys. Chem. B* **1997**, *101*, 3854−3871.
(14) Cleary, L.; Chen, H.; Chuang, C.; Silbey, R. J.; Cao, J. S. Optimal Fold Symmetry of LH2 Rings on a Photosynthetic Membrane. *Proc. Natl. Acad. Sci. U.S.A.* **2013**, *110*, 8537−8542.


DOI: 10.1021/acs.jpclett.5b00227
*J. Phys. Chem. Lett.* 2015, 6, 1240−1245

(15) Sumi, H. Theory on Rates of Excitation-Energy Transfer between Molecular Aggregates through Distributed Transition Dipoles with Application to the Antenna System in Bacterial Photosynthesis. *J. Phys. Chem. B* **1999**, *103*, 252−260.
(16) Scholes, G. D.; Fleming, G. R. On the Mechanism of Light Harvesting in Photosynthetic Purple Bacteria: B800 to B850 Energy Transfer. *J. Phys. Chem. B* **2000**, *104*, 1854−1868.
(17) Ma, J.; Cao, J. S. Förster Resonance Energy Transfer, Absorption and Emission Spectra in Multichromophoric Systems. I. Full Cumulant Expansions and System−Bath Entanglement. *J. Chem. Phys.* **2015**, *142*, 094106.
(18) Adolphs, J.; Renger, T. How Proteins Trigger Excitation Energy Transfer in the FMO Complex of Green Sulfur Bacteria. *Biophys. J.* **2006**, *91*, 2778−2797.
(19) Schmidt am Busch, M.; Müh, F.; El-Amine Madjet, M.; Renger, T. The Eighth Bacteriochlorophyll Completes the Excitation Energy Funnel in the FMO Protein. *J. Phys. Chem. Lett.* **2011**, *2*, 93−98.
(20) Novoderezhkin, V. I.; Palacios, M. A.; van Amerongen, H.; van Grondelle, R. Excitation Dynamics in the LHCII Complex of Higher Plants: Modeling Based on the 2.72Å Crystal Structure. *J. Phys. Chem. B* **2005**, *109*, 10493−10504.
(21) van Grondelle, R.; Novoderezhkin, V. I. Energy Transfer in Photosynthesis: Experimental Insights and Quantitative Models. *Phys. Chem. Chem. Phys.* **2006**, *8*, 793−807.
(22) Schlau-Cohen, G. S.; Calhoun, T. R.; Ginsberg, N. S.; Read, E. L.; Ballottari, M.; Bassi, R.; van Grondelle, R.; Fleming, G. R. Pathways of Energy Flow in LHCII from Two-Dimensional Electronic Spectroscopy. *J. Phys. Chem. B* **2009**, *113*, 15352−15363.
(23) Jesenko, S.; Žnidarič, M. Excitation Energy Transfer Efficiency: Equivalence of Transient and Stationary Setting and the Absence of Non-Markovian Effects. *J. Chem. Phys.* **2013**, *138*, 174103.
(24) Tanimura, Y.; Kubo, R. Time Evolution of a Quantum System in Contact with a Nearly Gaussian−Markoffian Noise Bath. *J. Phys. Soc. Jpn.* **1989**, *58*, 101−114.
(25) Moix, J.; Cao, J. S. A Hybrid Stochastic Hierarchy Equations of Motion Approach to Treat the Low Temperature Dynamics of Non-Markovian Open Quantum Systems. *J. Chem. Phys.* **2013**, *139*, 134106.
(26) Ai, Q.; Yen, T. C.; Jin, B. Y.; Cheng, Y. C. Clustered Geometries Exploiting Quantum Coherence Effects for Efficient Energy Transfer in Light Harvesting. *J. Phys. Chem. Lett.* **2013**, *4*, 2577−2584.
(27) Ishizaki, A.; Fleming, G. R. Theoretical Examination of Quantum Coherence in a Photosynthetic System at Physiological Temperature. *Proc. Natl. Acad. Sci. U.S.A* **2009**, *106*, 17255−17260.
(28) Renger, T.; Madjet, M. E.; Knorr, A.; Müh, F. How the Molecular Structure Determines the Flow of Excitation Energy in Plant Light-Harvesting Complex II. *J. Plant Physiol.* **2011**, *168*, 1497−1509.
(29) Kreisbeck, C.; Kramer, T.; Aspuru-Guzik, A. Scalable High-Performance Algorithm for the Simulation of Exciton Dynamics.Application to the Light-Harvesting Complex II in the Presence of Resonant Vibrational Modes. *J. Chem. Theory Comput.* **2014**, *10*, 4045−4054.
(30) The average error $\eta^{(h)}$ of the $h$th hierarchy order is defined using $\eta^{(h)} = 2\sum_{m\neq n} |k^{(h)}_{m\leftarrow n} - k^{(h-1)}_{m\leftarrow n}|/\sum_{m\neq n} |k^{(h)}_{m\leftarrow n}| + |k^{(h-1)}_{m\leftarrow n}|$, where $k^{(h)}_{m\leftarrow n}$ is the effective rate from site $n$ to site $m$ from the $h$th-order hierarchic expansion.
(31) Huo, P. F.; Coker, D. Theoretical Study of Coherent Excitation Energy Transfer in Cryptophyte Phycocyanin 645 at Physiological Temperature. *J. Phys. Chem. Lett.* **2011**, *2*, 825−833.
(32) Chuang, C.; Knoester, J.; Cao, J. S. Scaling Relations and Optimization of Excitonic Energy Transfer Rates between One-Dimensional Molecular Aggregates. *J. Phys. Chem. B* **2014**, *118*, 7827−7834.



DOI: 10.1021/acs.jpclett.5b00227
*J. Phys. Chem. Lett.* 2015, 6, 1240−1245